

Higher-Order Visualization of Causal Structures in Dynamics Graphs

Vincenzo Perri¹ and Ingo Scholtes²

Data Analytics Group
Department of Informatics (IfI)
University of Zurich
Zürich, Switzerland

¹perri@ifi.uzh.ch, ²scholtes@ifi.uzh.ch

Abstract

Graph drawing and visualisation techniques are important tools for the exploratory analysis of complex systems. While these methods are regularly applied to visualise data on complex networks, we increasingly have access to time series data that can be modelled as temporal networks or dynamic graphs. In such dynamic graphs, the temporal ordering of time-stamped edges determines the *causal topology* of a system, i.e. which nodes can directly and indirectly influence each other via a so-called *causal path*. While this causal topology is crucial to understand dynamical processes, the role of nodes, or cluster structures, we lack graph drawing techniques that incorporate this information into static visualisations. Addressing this gap, we present a novel dynamic graph drawing algorithm that utilises higher-order graphical models of causal paths in time series data to compute time-aware static graph visualisations. These visualisations combine the simplicity of static graphs with a time-aware layout algorithm that highlights patterns in the causal topology that result from the temporal dynamics of edges.

1 Introduction

Graph drawing and network visualisation techniques are an important methodological foundation for the exploratory analysis of data on complex systems. They help us to recognize patterns—such as, e.g., clusters or groups of well-connected nodes, hierarchical and core-periphery structures, or highly important nodes—in relational data on complex networks across disciplines [1, 2, 3, 4]. However, apart from data that capture which elements in a system are directly connected to each other, we increasingly have access to *time-stamped data* that additionally tell us at which time and in which chronological ordering those connections occur. Important examples from practice include time-stamped data on social interactions, financial transactions, passenger itineraries in transportation networks, click stream data in the web, or gene regulatory interactions [5].

Despite these important applications, the visualisation of *dynamic graph* or *temporal network* data is still a challenge [6, 7]. Common approaches to visualise dynamic graphs animate the evolution of the topology as sequences of static snapshots, where each snapshot is a graph representing the connections active at a given point in time or within a certain time interval. Such animations can help us to gain a high-level understanding of temporal activities in dynamic graphs. However, they are cognitively demanding and complex, which makes it hard to recognize patterns that determine how the nodes in a graph influence each other over time. Moreover, for high-resolution time-stamped data, where only one or few interactions occur at any given time stamp, the application of graph drawing algorithms to temporal snapshot graphs necessitates a coarse graining of time. This introduces a major issue: we lose information on the chronological ordering of links that determines so-called *time-respecting* or *causal paths* [8, 5]. In a nutshell, for two time-stamped edges $(a, b; t_1)$ and $(b, c; t_2)$ occurring at times t_1 and t_2 a *causal path* \overrightarrow{abc} from node a via node b to node c can

only exist if edge (a, b) occurs before edge (b, c) , i.e. if $t_1 < t_2$. If the chronological ordering of edges is reversed, such a causal path does not exist, i.e. in this case node a cannot (indirectly) influence node c via b .

This simple example highlights an important issue of (static) graph models of time series data. While two edges (a, b) and (b, c) in a static graph imply that a (transitive) path \overrightarrow{abc} exists, the temporal ordering of time-stamped edges in dynamic graphs can invalidate this assumption. A number of empirical works have shown that the complex chronological orderings in which time-stamped edges occur in real time series data gives rise to surprisingly complex causal paths. This has important implications for the modelling of epidemic processes, for random walk and diffusion dynamics, centrality measures used to rank nodes and predict influential users in social networks, as well as clustering techniques commonly applied in social network analysis or recommender systems. In a nutshell, the temporal ordering of edges in real dynamic graphs gives rise to complex *causal topologies* that invalidate standard graph models and call for a new class of higher-order network modelling, analysis, and visualisation techniques [9]. So far, most dynamic graph drawing techniques have neglected the effect of the chronological ordering of interactions on a system's causal topology. In a recent review summarising the state-of-the-art in temporal network analysis [7], Holme points out a lack of visualisation techniques that (i) go beyond cognitively demanding animations, and (ii) consider the complex topology of causal paths in high-resolution time series data. He argues that

"[. . .] temporal networks lack the intuitive visual component of static networks. Probably this is a fundamental property that cannot be completely altered, but there should be better visualization methods than we have now. Highest on our wish list is a method that both simplifies some structures and keeps (at least some) of the time-respecting paths (maybe at the cost of not having time on the abscissa)." [7], p. 23

Addressing this gap, we develop a novel visualisation approach that incorporates information on causal paths in dynamic graphs into simple (static) graph visualisations. Our contributions are:

- We highlight a lack of time-aware graph visualisation techniques that respects the *causal topology* resulting from the chronological ordering of edges in high-resolution data on dynamic graphs.
- We develop a dynamic graph drawing algorithm that generalises force-directed layouts to high-dimensional De Bruijn graph models of causal paths [10, 11]. Our algorithm incorporates multiple higher-order models up to a maximum order that can be determined through principled model selection techniques.
- We quantitatively assess the quality of time-aware visualisations both in synthetic and empirical data on dynamic graphs. The results show that that our approach helps to (i) detect clusters of vertices that are well-connected via causal paths but invisible in standard graph drawing techniques, and (ii) identify important vertices with high temporal centrality.
- We provide an Open Source `python` implementation of our algorithm [12]. It can be used to visualise dynamic graphs from different sources, including, e.g., time-stamped social interactions, user click streams on the Web, or passenger itineraries in transportation networks.

Focusing on time-aware static visualisations that highlight temporal patterns neglected by existing techniques, we take a new approach to dynamic graph drawing. Generalising layout algorithms to De Bruijn graph models commonly used in bioinformatics [13], we further uncover a relation between data structures used in biological sequence mining and (dynamic) graph drawing. Considering recent works on learning optimal higher-order graph models from rich time series data [11], our work further opens interesting perspectives to combine machine learning and graph drawing.

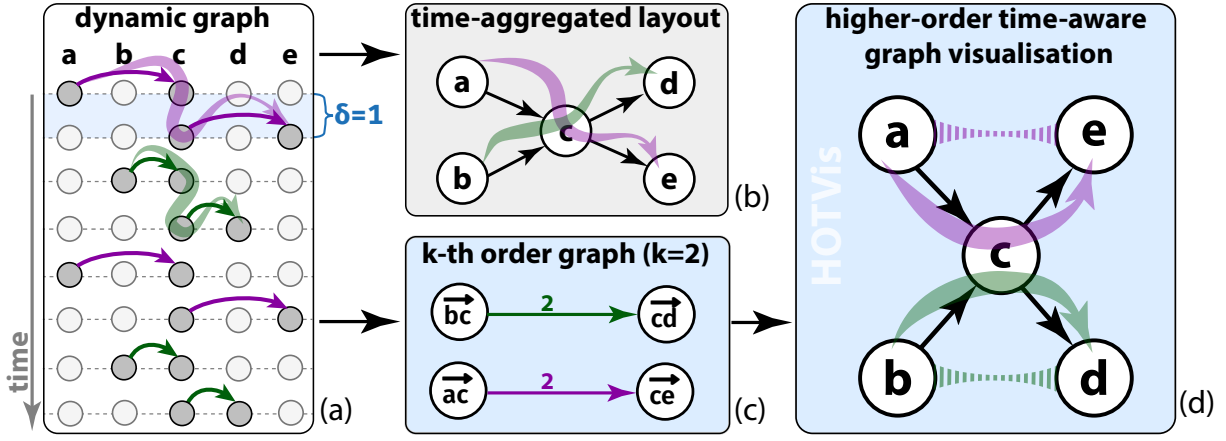


Figure 1: Standard time-aggregated visualisations (b) discard information on *causal paths* (coloured arrows) in a dynamic graph (a). HOTViS uses higher-order graph models of causal paths (c) to produce time-aware, static visualisations (d) that highlight the causal topology of dynamic graphs.

2 Preliminaries and Related Work

In the following we formally define dynamic graphs and causal paths and highlight the research gap that motivates our work through a review of related works.

2.1 Dynamic graphs and causal paths

We define a dynamic graph as a tuple $G^{(t)} = (V, E^{(t)})$, where V is a set of vertices and $E^{(t)}$ is a set of time-stamped edges $E^{(t)} \subseteq V \times V \times \mathbb{N}$. We assume that $(v, w; t) \in E_t$ denotes that a directed edge between source vertex v and target vertex w occurred *instantaneously* at discrete time $t \in \mathbb{N}$. We further say that a (static) graph $G = (V, E)$ is the *time-aggregated graph* corresponding to a dynamic graph $G^{(t)}$ iff $(v, w) \in E \leftrightarrow \exists t \in \mathbb{N} : (v, w; t) \in E^{(t)}$. We further assume that the edge weights $w : E \rightarrow \mathbb{N}$ of such a time-aggregated graph capture the number of times edges have been active in the corresponding dynamic graph, i.e. we define $w(v, w) := |\{t \in \mathbb{N} : (v, w; t) \in E^{(t)}\}|$. A simple example for a dynamic graph with eight time-stamped edges and five nodes is shown in fig. 1 (a).

A key concept in the study of patterns and processes in dynamic graphs is that of a *time-respecting* or *causal path* [8, 5, 14]. For a given dynamic graph $G = (V, E^{(t)})$ we call a sequence $(v_0, v_1, t_0), (v_1, v_2, t_1), \dots, (v_{l-1}, v_l, t_l)$ of time-stamped edges a *causal path* $p = \overrightarrow{v_0 v_1 v_2 \dots v_l}$ of length l from vertex v_0 to v_l iff (i) $(v_i, v_{i+1}; t_i) \in E_{t_i}$, and (ii) $0 < t_{i+1} - t_i \leq \delta$ holds for $i \in \{0, 1, \dots, l-1\}$. We thus define the length of causal paths as the number of edges that they traverse, which implies that each time-stamped edge is a causal path of length one. In this definition, the condition $0 < t_{i+1} - t_i$ ensures that the sequence of time-stamped edges respects the “arrow of time”. The condition $t_{i+1} - t_i \leq \delta$ additionally allows us to consider a *time scale* that defines up to which temporal distance two consecutive edges are considered to contribute to a causal path. For a maximum value of $\delta = \infty$, we obtain a definition of causal paths that is purely based on the chronological ordering of edges, while for $\delta < \infty$ we additionally assume that vertices have a maximum “memory” of δ time units within which they can pass information along causal paths. We illustrate this definition in fig. 1 (a) for $\delta = 1$, where the two resulting causal paths $\overrightarrow{ac\bar{e}}$ and $\overrightarrow{bc\bar{d}}$ of length two (each occurring twice) are highlighted. While the detection of the “optimal” time scale δ for the definition of causal paths in a given dynamic graph is beyond the scope of our work, this problem is closely related to the question of finding the optimal window size in temporal network analysis [15].

We note that the existence of a causal path $\overrightarrow{v_0 \dots v_l}$ is a necessary condition for a vertex v_0 in a dynamic graph to *causally influence* another vertex v_l . We further observe that each causal path

in $G^{(t)}$ necessarily implies that the same path exists in the time-aggregated graph G . Conversely, the existence of a path in the time-aggregated graph G corresponding to the dynamic graph $G^{(t)}$ does *not* imply that the corresponding causal path exists in $G^{(t)}$. This is due to the fact that the time-aggregated graph G is a static projection of the dynamic graph $G^{(t)}$ along the time axis, which discards all information on the time dimension. This is illustrated in fig. 1 (b), where the two paths \overrightarrow{acd} and \overrightarrow{bce} in the *static* have no equivalent in terms of a *causal path* in the dynamic graph shown in fig. 1 (a). This has the important implication that the chronological order of edges in *dynamic* graphs can invalidate the *transitivity of paths*, which—through algebraic operations on adjacency matrices—is deeply enshrined into the mathematical foundation of graph theory [9]. The example in fig. 1 (a) illustrates how the chronological order of edges can break transitivity in a dynamic graph. Here, the timing and ordering of time-stamped edges implies that only two of the four theoretically possible *causal paths* of length two exist. This implies that, despite the presence of corresponding paths in the static topology, vertices a and b cannot indirectly influence d and e via causal paths \overrightarrow{acd} and \overrightarrow{bce} respectively.

2.2 Dynamic Graph Drawing

Having motivated the effects that are due to the arrow of time in dynamic graphs, we review related works on dynamic graph drawing. Using the taxonomy from [16], we categorize those works in (i) animation techniques that map the time dimension of dynamic graphs onto a time dimension of the resulting visualisation, and (ii) time-line representations that map the temporal evolution of dynamic graphs to a spatial dimension. We present methods only insofar as they are relevant to our work, while referring the reader to [6, 16] for a detailed review.

Animated visualisations of dynamic graphs. A natural approach to visualise time series data on graphs are animated, “movie”-like visualisations that show the temporal evolution of vertices and/or edges. To generate such animations, we need to create a sequence of graph visualisations, where each graph is a *snapshot* of the vertices and edges that exist at a particular point in time. An intuitive benefit of this approach is that we can — at least as a first approximation — reduce the problem of drawing a *dynamic* graph to the (simpler) problem of drawing a sequence of *static* graphs. A common approach to draw static graphs is through layout algorithms, that use the graph topology to map vertices to coordinates in two-dimensional Euclidean space such that a graph’s inherent structures and symmetries become visible [1, 17, 18, 19, 20]. A naive application of those methods to multiple snapshots of dynamic graphs is likely to result in animations that make it difficult to associate structures in subsequent frames, a problem often framed as maintaining the user’s “mental map” of a graph [21, 22, 23]. A large number of works have thus focused on methods to optimize graph layouts across multiple snapshots [24, 25, 26, 27, 28, 29, 30, 31, 32, 33], or to generate smooth transitions [34, 35, 36] that minimize the cognitive effort required to trace time-varying vertices, edges, or clusters through subsequent snapshots.

Animations beyond Time-Slice Graphs. Apart from the issue that animations are cognitively demanding, additional challenges arise in data with high temporal resolution (e.g. seconds or even millisecond), where a single vertex or edge is likely to be active in each time stamp. The application of static graph drawing techniques to such data requires a coarse-graining of time into *time-slices*, such that each time slice gives rise to a graph snapshot that can be visualised using, e.g., force-directed layout algorithms. As pointed out in [37], this coarse-graining of time into time slices leads to a loss of information on causal paths and few dynamic graph drawing techniques have specifically addressed this issue.

Timeline representations. Despite the advances outlined above, recognizing patterns in animation-based visualisations of dynamic graphs remains a considerable cognitive challenge for users. Moreover, it is difficult to embed dynamic graph animations into scholarly articles, books, or posters, which often limits their use in science and engineering to illustrative supplementary material. Addressing these issues, a second line of research focuses on methods to visualize dynamic graphs in terms of *timeline representations*, which map the time dimension of dynamic graphs to a spatial dimension that can be embedded into a static visualisation. Examples includes widely-used directed acyclic of time-unfolded graph representations of dynamic graphs [8, 38], *time arc* or *time radar trees* [39, 40, 41], sequences of layered adjacencies [42], stacked 3D representations where consecutive time slices are arranged along a third dimension [25]. While recent works have proposed circular representations that scale to larger time series [43], the application of visualisations that map time to a spatial dimension is limited to a moderately large number of time stamps. Moreover, to the best of our knowledge, the effects of the chronological order of edges on the causal topology has not been considered in static visualisations of dynamic graphs.

3 Higher-Order Time-Aware Visualisation of Graphs

To address the issues outlined in section 2, we propose a new approach to draw dynamic graphs that neither generates animated sequences of static snapshots, nor explicitly maps the time dimension of dynamic graphs to an additional spatial dimension. We instead apply a well-known layout algorithm to generalised graph models that capture how the temporal dimension of the dynamic graph influences its causal topology, i.e. which vertices can influence each other via causal paths. Our goal is to preserve temporal-topological patterns hidden in the time dimension of dynamic graphs and use them in the layout of a time-aggregated graph. We obtain a *time-aware static visualisation* that can be intuitively interpreted in analogy to standard static graph layouts. A maximally simple illustration of such a time-aware visualisation is shown in fig. 1 (d), where—different from fig. 1 (b)—the fact that vertex a can influence vertex e and vertex b can influence vertex d via a causal path is reflected in the positioning of vertices.

Using a perspective recently developed in the network science community [9], our method is based on a generalisation of a time-aggregated graphs to *higher-order graph models* that capture causal paths in time-stamped network data. While different approaches like memory networks [44], variable-order state-space extensions [45], multiplex network representations [46], temporal event graphs [47, 48], or simplicial complexes [49] have been proposed, here we adopt the higher- and multi-order modelling framework developed in [50, 51, 11]. It generalises time-aggregated graphs to higher-order models that resemble *k-dimensional De Bruijn graphs* [10, 11]. For a given dynamic graph $G^{(t)}$ and order $k \geq 1$ we define a *higher-order graph* $G^{(k)}$ as tuple $G^{(k)} = (V^{(k)}, E^{(k)})$ of higher-order vertices $V^{(k)} \subseteq V^k$ and higher-order edges $E^{(k)} \subseteq V^{(k)} \times V^{(k)}$. Each higher-order vertex $v =: \overrightarrow{v_0 v_1 \dots v_k} \in V^{(k)}$ is an ordered tuple of k vertices $v_i \in V$ in the dynamic graph $G^{(t)}$. Adopting the iterative line graph construction of high-dimensional De Bruijn graphs [10], we further restrict edges $E^{(k)}$ of a k -th order graph to connect higher-order vertices that overlap in exactly $k - 1$ vertices, i.e. we require

$$(\overrightarrow{v_0 v_1 \dots v_{k-1} v_k}, \overrightarrow{w_0 w_1 \dots w_{k-1} w_k}) \in E^{(k)} \Rightarrow v_i = w_{i-1} \text{ for } i = 1, \dots, k$$

Utilising the modelling framework introduced in [50, 51, 11] we can use (weighted) higher-order edges of a k -th order graph $G^{(k)}$ to represent the frequency of causal paths of length k in a dynamic graph, i.e we define weights $w : E^{(k)} \rightarrow \mathbb{N}$ as

$$w(\overrightarrow{v_0 \dots v_k}, \overrightarrow{v_1 \dots v_k}) := |(t_0, \dots, t_{k-1}) : (e; t_i) \in E^{(t)} \text{ form causal path } \overrightarrow{v_0 \dots v_k}|$$

Hence, the weight of edge $(\overrightarrow{v_0 \dots v_k}, \overrightarrow{v_1 \dots v_k})$ in a k -th order graph $G^{(k)}$ counts how often a causal path $\overrightarrow{v_0 \dots v_k}$ of length k occurs in the dynamic graph $G^{(t)}$. Figure 1 (c) shows an example for a

(trivial) higher-order graph model of order $k = 2$ that represents the causal paths \overrightarrow{bcd} and \overrightarrow{ace} of length two in the dynamic graph in fig. 1 (a).¹

Higher-order graphs naturally generalise time-aggregated graph representations of dynamic graphs, where for $k = 1$ we have $V^{(1)} = V$ and $E^{(1)} = E$. Hence, a weighted time-aggregated graph is a first-order model of a dynamic graph that counts edges, i.e. causal paths of length one. For $k > 1$, we obtain higher-order models that capture both the topology and the chronological ordering of time-stamped edges in a dynamic graph, where the second-order model is the simplest model that is sensitive to the timing and ordering of time-stamped edges. Despite the simplicity of this construction, higher-order models of causal paths have led to rich insights into empirical dynamic graphs. They help us to understand how correlations affect epidemic spreading [38], give rise to spectral measures that can be used to predict the speed-up or slow-down of diffusion processes due to the temporal ordering of edges [50], are the basis for time-aware vertex centrality measures [51], improve the ranking of web pages with click stream data [11], enable anomaly detection in time series data [53], and yield insights into temporal patterns in the careers of scientists[54]. Highlighting a novel application area, we show that higher-order graphs can be used to visualise the causal topology of dynamic graphs. Our algorithm to generate higher-order time-aware visualisations (HOTVis) generalises the force-directed layout algorithm introduced in [19] to high-dimensional De Bruijn graphs. Force-directed layouts are a popular class of physics-inspired graph layout algorithms. They address the problem of optimally positioning vertices in a Euclidean space by means of a many-body simulation. To ensure that vertices connected by an edge are placed in close proximity, they introduce attractive forces that act between the endpoints of edges. Additional repulsive forces are simulated to between all vertices in order to separate them. Iteratively simulating those forces until an equilibrium state is reached leads to layouts that highlight structures and symmetries in a graph [1].

Like other network analysis and graph mining techniques, force-directed layout algorithms implicitly rely on the assumption that paths in a graph are transitive, which can be invalidated by the ordering of edges in a dynamic graph [9]. In particular, for two edges (a, b) and (b, c) , the attractive forces acting between vertex pairs a, b and b, c are likely to yield a layout in which vertices a and c are placed in close proximity. For time-aggregated, static layouts of dynamic graphs, this positioning of vertices does not consider whether the vertices a and c can influence each other via a causal path, thus producing visualisations that do not respect the *causal topology* of a dynamic graph (see fig. 1 (b)). Addressing this issue, HOTVis generalises attractive forces to higher-order graphs that capture the topology of causal paths in time-stamped data. In particular, our algorithm *superimposes* attractive forces that act between the endpoints of edges in multiple higher-order graph models up to a configurable maximum order K . Figure 1 (d) illustrates this idea based on the edges in the second-order model shown in fig. 1 (c). The additional attractive forces between vertex pairs a, e and b, d (coloured lines in fig. 1 (d)) change the positioning of vertices such that those vertices that can causally influence each other are positioned in proximity.

The pseudocode of HOTVis is shown in Algorithm 1. It takes a dynamic graph $G^{(t)}$, a maximum time difference δ used to define causal paths, a maximum order K , a number of iterations N , and parameters α_k that control how much paths of length k influence the layout. The algorithm consists of two phases. In a first phase, higher-order graphs $G^{(k)}$ up to order K are generated as described above (lines 4–5). For each edge $(\overrightarrow{v_0 \dots v_{k-1}}, \overrightarrow{v_1 \dots v_k})$ in $G^{(k)}$, an attractive force between vertices v_0 and v_k that can influence each other via causal path $\overrightarrow{v_0 v_1 \dots v_k}$ is added (lines 7–10). The strength of this force depends on (i) the frequency of the corresponding causal path, and (ii) a parameter α_k that controls the influence of causal paths of length k on the generated time-aware layout. For $\alpha_2 = \dots = \alpha_K = 0$ we obtain a standard force-directed (first-order) layout in which time is ignored. For $\alpha_k > 0$ for $k > 1$ vertex positions are additionally influenced by the chronological ordering of time-stamped edges. In a second phase of HOTVis (lines 11–22), we use the heuristic many-body simulation proposed by Fruchterman and Reingold [19] to iteratively simulate the superimposed

¹Note that for any given maximum time difference δ the causal paths of any length k can be counted efficiently in large time series data on graphs [52].

attractive forces and additional repulsive forces between all pairs of vertices. The algorithm returns a dictionary of vertex positions Pos that can be used to generate a static graph visualisation.

Algorithm 1 HOTVis: Higher-order time-aware layout with max. order K

```

1: procedure HOTVis( $G^{(t)}, K, N, \delta, \alpha_2, \dots, \alpha_K$ )
2:    $A, \text{Pos} = \text{dict}()$ 
3:    $\text{Temp} = t_0$ 
4:   for  $k \in \text{range}(1, K)$  do                                      $\triangleright$  superimpose attractive forces
5:      $G^{(k)} = \text{HigherOrderGraph}(G^{(t)}, \delta, k)$ 
6:     for  $(\overrightarrow{v_0 \dots v_{k-1}}, \overrightarrow{v_1 \dots v_k}) \in E^{(k)}$  do
7:       if  $(v_0, v_k) \in A$  then
8:          $A[v_0, v_k] = A[v_0, v_k] + \alpha_k \cdot w(\overrightarrow{v_0 \dots v_{k-1}}, \overrightarrow{v_1 \dots v_k})$ 
9:       else
10:         $A[v_0, v_k] = \alpha_k \cdot w(\overrightarrow{v_0 \dots v_{k-1}}, \overrightarrow{v_1 \dots v_k})$ 
11:    for  $i \in \text{range}(N)$  do                                        $\triangleright$  apply many-body simulation [19]
12:      for  $v \in V$  do
13:         $\Theta = 0$ 
14:        for  $w \in V, w \neq v$  do
15:           $\Delta = \text{Pos}[w] - \text{Pos}[v]$ 
16:           $\Theta = \Theta - \Delta/|\Delta| \cdot k^2/|\Delta|$ 
17:        for  $(v, w) \in A$  do
18:           $\Delta = \text{Pos}[w] - \text{Pos}[v]$ 
19:           $\Theta = \Theta + \Delta/|\Delta| \cdot A[v, w] \cdot |\Delta|^2/k$ 
20:         $P[v] = P[v] + \Theta/|\Theta| \cdot \min(|\Theta|, \text{Temp})$ 
21:       $\text{Temp} = \text{cool}(\text{Temp})$ 
return  $\text{Pos}$ 

```

Illustration in synthetic example A demonstration of a time-aware visualisation of a synthetically generated dynamic graph with $K = 2$ is shown in Figure 1. This dynamic graph was generated from

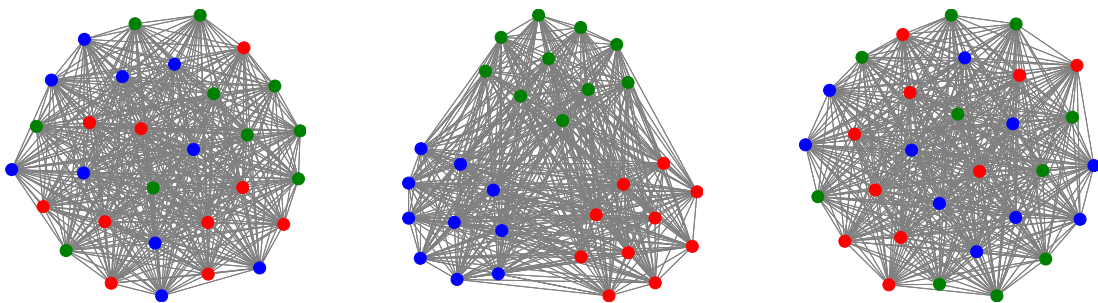


Figure 2: Application of HOTVis to synthetic dynamic graph with three temporal clusters (coloured nodes, see details in appendix A). A second-order time-aware layout (middle) clearly represents cluster structures not visible in a standard (first-order) layout (left). A time-aware visualisation of the same data with randomly shuffled time stamps (right) confirms that clusters are solely due to the chronological ordering of edges.

a stochastic model that generates edge sequences with temporal correlations that lead to an over-representation of causal paths with length two that (indirectly) connect pairs of vertices within three clusters (coloured vertices in fig. 2), where each cluster consists of ten vertices. We highlight that those *temporal clusters* in the *causal topology* of the dynamic graph cannot be detected based on the random k -regular topology of the time-aggregated static graph. A description of the model is included in appendix A and an animation of the dynamic graph is available in the supplementary

material. Figure 2 (a) shows a standard (first-order) force-directed layout that ignores the time dimension of the underlying dynamic network. In contrast, Figure 2 (b) shows a second-order time-aware visualisation that superimposes attractive forces calculated in both the first and the second-order graph. As a result, the three *temporal clusters* are clearly highlighted in the placement of vertices. We finally randomly shuffle the time stamps of edges to destroy temporal correlations in the chronological ordering of edges and recompute the second-order time-aware layout for the (shuffled) dynamic graph. Due to this shuffling, causal paths in the (randomised) causal topology are likely to correspond to paths in a static time-aggregated graph,. The time-aware visualisation of this shuffled dynamic graph in fig. 2 (c) closely resembles the standard graph layout, which confirms that our algorithm emphasises patterns that are due to the time dimension of dynamic graphs.

4 Experimental Evaluation

Having described and illustrated HOTVis, we now experimentally evaluate whether the obtained visualizations better represent the causal topology of dynamic graphs. For this we use quantitative *layout quality* measures, which we define in appendix B and, due to space constraints, only briefly explain in the following.

Layout Quality Measures. As a first measure for layout quality, we calculate the **edge crossing** (ξ), which counts pairs of edges that cross each other. It captures the idea that “high-quality” drawings of (non-planar) graphs should minimise ξ , since a large number of edge crossings makes it difficult to identify vertices connected by edges [1]. Accounting for the causal topology of dynamic graphs, we generalise this measure to **path crossing** (Ξ), which counts pairs of *causal paths* of any length that “cross” each other. While referring to appendix B for a formal definition, fig. 1(b) shows a layout where two causal paths $\vec{ac\hat{e}}$ and $\vec{bc\hat{d}}$ cross each other in c , while they do not in fig. 1(d). This measure is motivated by the idea that high-quality *time-aware* layouts should position vertices such that causal paths can be followed along edges while crossing a minimal number of unrelated causal paths. Finally, above we have argued that—due to the transitivity of paths in static graphs—force-directed layouts position vertices that directly or indirectly influence each other via short paths in proximity. To capture the more complex notion of indirect influence via causal paths in dynamic graphs, we define **causal path dispersion** (σ) (see appendix B). For a set of causal paths $p = \vec{v_0 \dots v_l}$ we define σ as the average distance of vertices v_i traversed by p from the barycentre of those vertices v_i . We further normalise σ such that we obtain $\sigma = 1$ if the positions of vertices traversed by causal paths are randomly distributed across the visualisation. σ measures the spatial dispersion of those vertices that can causally influence each other via causal paths. We expect a high-quality time-aware layout to position vertices that are connected by many causal paths close to each other and thus aim for small values of σ .

Experimental results. We first use these measures to assess time-aware layouts for the synthetic dynamic graph with three clusters introduced in section 3. The results are shown in the left column of fig. 3. The edge crossing ξ increases by approx. 1% from first to second order and remains stable for $K > 2$. Conversely, the time-aware layout improves the path crossing Ξ by approx. 50% while σ improves by 9% for $K > 1$. We next consider empirical data capturing face-to-face interactions between humans equipped with wearable sensors [55]. The first data set, `hospital`, captures 32,424 time-stamped proximity events between 75 patients, medical and administrative staff in a hospital recorded over a period of five days [56]. The second data set, `workplace`, captures 9,827 face-to-face interactions between 92 company employees recorded in an office building over a period of ten days [57]. The results for those data sets are shown in the middle and right column of fig. 3. As expected, the number of edge crossings ξ increases with K for both cases, while the number of path crossings Ξ decreases. The largest drop in the path crossing Ξ is observed for $K = 2$ with -7% and -36% for `hospital` and `workplace`. This is accompanied by an increase of edge crossing ξ of

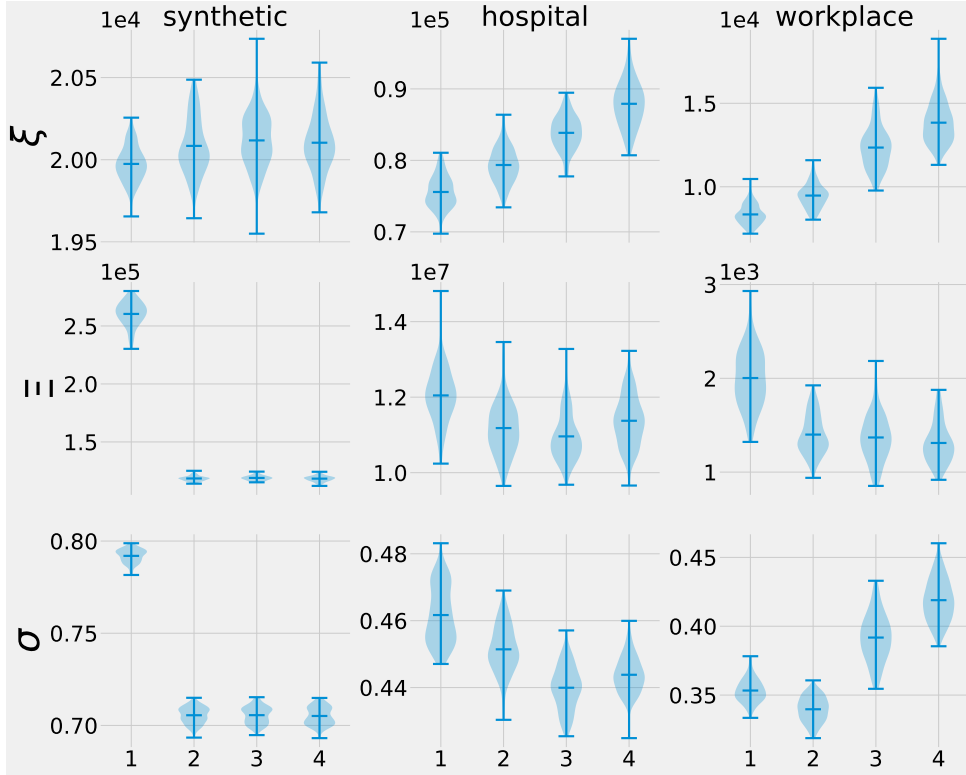


Figure 3: Evaluation of edge crossing (ξ , top row), causal path crossing (Ξ , middle row), and causal path dispersion (σ , bottom row) for a synthetic dynamic graph with three clusters (left) and empirical data on time-stamped interactions between patients and hospital staff (middle) and workers in an office environment (right). Values are averages of 100 cross-validation experiments, where a time-aware layout with maximum order K (x-axis) is computed for a 30% random training set of causal paths, calculating quality measures (y-axis) for generated layouts in a test set of remaining 70% of causal paths.

5% and 14% respectively. For causal path dispersion σ the two data sets show different trends: For *hospital* σ decreases at $K = 2$ and remains small for $K > 2$ while for *workplace* the decrease at $K = 2$ is followed by an increase in the third and fourth order.

These results support our hypothesis that HOTOVis better represents the causal topology of dynamic graphs (in terms of Ξ and σ) compared to first-order layouts. For a suitably chosen order K , we find that a large decrease of Ξ and σ is linked to a relatively mild increase of ξ . On the one hand, this supports our claim that HOTOVis improves the visualisation of causal topologies. On the other hand, this raises the issue of finding the “optimal” order K of a higher-order graph model. We emphasize that (i) this issue can be addressed using a statistical model selection technique [11], and (ii) in agreement with our results this technique yields an optimal order two for all three data sets.

Temporal closeness. In force-directed layouts, vertices at short topological distance tend to be positioned close to each other. This implies that vertices that are topologically close to many other vertices, i.e. vertices with high closeness centrality, are preferentially positioned close to the centre of the visualization. However, the time dimension of dynamic graphs can alter causal paths and thus the *temporal closeness* of vertices compared to the static graph topology [14, 51]. While this is not reflected in standard (time-ignoring) static visualisations, an interesting question is whether HOTOVis places vertices with high temporal closeness centrality in the centre of the visualization. We evaluate this by calculating **closeness eccentricity** Δ , which captures the sum of distances from the barycenter of vertex positions for n vertices with highest temporal closeness centrality [14, 51]. Referring to appendix B for details, the measure is normalized such that values larger or smaller than

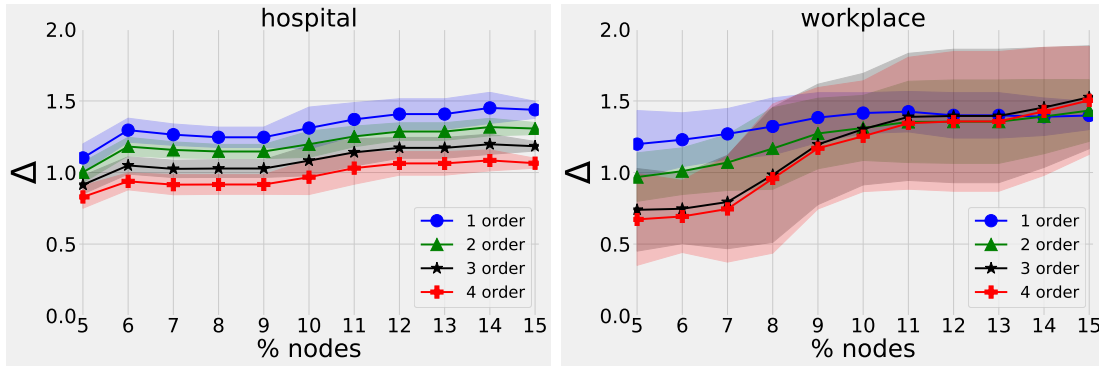


Figure 4: Closeness eccentricity Δ (y-axis) for a varying top percentage n of vertices with highest temporal closeness (x-axis). Results are shown for empirical data on time-stamped interactions in a hospital (left) and workers in an office environment (right) and different max. order K (coloured hull curves) of a higher-order time-aware layout.

one capture whether the most central vertices are closer ($\Delta < 1$) or farther away ($\Delta > 1$) from the centre than expected at random. The results for the two empirical data sets are shown in fig. 4 (again for 100 cross-validation experiments). For $K = 1$ we find $\Delta > 1$ for both data sets, which shows that the temporal closeness of vertices is not well-represented in a standard time-aggregated visualisation. For $K > 1$ HOTVis outperforms a first-order layout in both data sets, with Δ decreasing for growing values of K .

5 Conclusion and Outlook

Despite advances in graph drawing, the visualisation of high-resolution time-stamped network data is still a challenge. Existing methods have either visualised dynamic graphs as animations or map time to a spatial dimension. They suffer from their limited ability to highlight patterns in the *causal topology of dynamic graphs*, which is determined by the interplay between its topology (i.e. *which edges exist*) and the temporal dynamics of edges (i.e. *when time-stamped edges occur*). We address this issue through HOTVis, a dynamic graph drawing algorithm that uses higher-order graph models to produce static, time-aware visualisations. Experiments in synthetic and empirical dynamic graphs support our hypothesis that the resulting visualisations highlight temporal clusters and temporal vertex centralities. Our work opens perspectives for a new class of time-aware static visualisations that benefit from advances in the statistical modelling of higher-order structures in dynamic graphs. Referring to recently developed statistical methods to learn *optimal higher-order graph representations* for time series data [11, 45, 58, 9], our work creates interesting opportunities to combine machine learning and graph drawing that we will explore in the future.

Acknowledgements

The authors acknowledge financial support by the Swiss National Science Foundation (SNSF) via grant no. 176938. The authors further acknowledge feedback by Luka Petrović on a draft of the manuscript.

References

- [1] Di Battista, G., Eades, P., Tamassia, R. & Tollis, I. G. Algorithms for drawing graphs: an annotated bibliography. *Computational Geometry* **4**, 235–282 (1994).
- [2] Herman, I., Melancon, G. & Marshall, M. S. Graph visualization and navigation in information visualization: A survey. *IEEE Transactions on Visualization and Computer Graphics* **6**, 24–43 (2000).
- [3] Kaufmann, M. & Wagner, D. *Drawing graphs: methods and models*, vol. 2025 (Springer, 2003).
- [4] Noguchi, C. & Kawamoto, T. Evaluating network partitions through visualization. *arXiv e-prints* arXiv:1906.00699 (2019). 1906.00699.
- [5] Holme, P. & Saramäki, J. Temporal networks. *Phys. Rep.* **519**, 97 – 125 (2012). URL <http://www.sciencedirect.com/science/article/pii/S0370157312000841>.
- [6] Beck, F., Burch, M., Diehl, S. & Weiskopf, D. The state of the art in visualizing dynamic graphs. *EuroVis STAR* **2**, 1–21 (2014).
- [7] Holme, P. Modern temporal network theory: a colloquium. *The European Physical Journal B* **88**, 234 (2015).
- [8] Kempe, D., Kleinberg, J. & Kumar, A. Connectivity and inference problems for temporal networks. In *Proceedings of the thirty-second annual ACM symposium on Theory of computing*, 504–513 (ACM, 2000).
- [9] Lambiotte, R., Rosvall, M. & Scholtes, I. From networks to optimal higher-order models of complex systems. *Nature physics* **1** (2019).
- [10] De Bruijn, N. G. A combinatorial problem. *Koninklijke Nederlandse Akademie v. Wetenschappen* **49**, 758–764 (1946).
- [11] Scholtes, I. When is a network a network?: Multi-order graphical model selection in pathways and temporal networks. In *Proceedings of the 23rd ACM SIGKDD International Conference on Knowledge Discovery and Data Mining, Halifax, NS, CA, August 2017*, KDD '17, 1037–1046 (ACM, New York, NY, USA, 2017). URL <http://doi.acm.org/10.1145/3097983.3098145>. <http://doi.acm.org/10.1145/3097983.3098145>.
- [12] Scholtes, I. pathpy software package. <https://github.com/IngoScholtes/pathpy> (2017). [Online].
- [13] Chikhi, R., Limasset, A., Jackman, S., Simpson, J. T. & Medvedev, P. On the representation of de bruijn graphs. In Sharan, R. (ed.) *Research in Computational Molecular Biology*, 35–55 (Springer International Publishing, Cham, 2014).
- [14] Pan, R. & Saramäki, J. Path lengths, correlations, and centrality in temporal networks. *Phys. Rev. E* **84**, 1–10 (2011).
- [15] Krings, G., Karsai, M., Bernhardsson, S., Blondel, V. & Saramäki, J. Effects of time window size and placement on the structure of an aggregated communication network. *EPJ Data Science* **1** (2012). URL <http://dx.doi.org/10.1140/epjds4>.
- [16] Beck, F., Burch, M., Diehl, S. & Weiskopf, D. A taxonomy and survey of dynamic graph visualization. *Computer Graphics Forum* **36**, 133–159 (2017). URL <https://onlinelibrary.wiley.com/doi/abs/10.1111/cgf.12791>. <https://onlinelibrary.wiley.com/doi/pdf/10.1111/cgf.12791>.

- [17] Eades, P. A heuristic for graph drawing. *Congressus numerantium* **42**, 149–160 (1984).
- [18] Kamada, T., Kawai, S. *et al.* An algorithm for drawing general undirected graphs. *Information processing letters* **31**, 7–15 (1989).
- [19] Fruchterman, T. M. & Reingold, E. M. Graph drawing by force-directed placement. *Software: Practice and experience* **21**, 1129–1164 (1991).
- [20] Hu, Y. Efficient, high-quality force-directed graph drawing. *Mathematica Journal* **10**, 37–71 (2005).
- [21] Coleman, M. K. & Parker, D. S. Aesthetics-based graph layout for human consumption. *Software: Practice and Experience* **26**, 1415–1438 (1996).
- [22] Purchase, H. C., Hoggan, E. & Görg, C. How important is the “mental map”?—an empirical investigation of a dynamic graph layout algorithm. In *International Symposium on Graph Drawing*, 184–195 (Springer, 2006).
- [23] Archambault, D. W. & Purchase, H. C. Mental map preservation helps user orientation in dynamic graphs. In *Graph Drawing - 20th International Symposium, GD 2012, Redmond, WA, USA, September 19-21, 2012, Revised Selected Papers*, 475–486 (2012). URL https://doi.org/10.1007/978-3-642-36763-2_42.
- [24] Diehl, S., Görg, C. & Kerren, A. Preserving the mental map using foresighted layout. In *Data Visualization 2001*, 175–184 (Springer, 2001).
- [25] Erten, C., Kobourov, S. G., Le, V. & Navabi, A. Simultaneous graph drawing: Layout algorithms and visualization schemes. In *International Symposium on Graph Drawing*, 437–449 (Springer, 2003).
- [26] Görg, C., Birke, P., Pohl, M. & Diehl, S. Dynamic graph drawing of sequences of orthogonal and hierarchical graphs. In *International Symposium on Graph Drawing*, 228–238 (Springer, 2004).
- [27] Frishman, Y. & Tal, A. Online dynamic graph drawing. *IEEE Transactions on Visualization and Computer Graphics* **14**, 727–740 (2008).
- [28] Hurter, C., Ersoy, O., Fabrikant, S. I., Klein, T. R. & Telea, A. C. Bundled visualization of dynamicgraph and trail data. *IEEE transactions on visualization and computer graphics* **20**, 1141–1157 (2014).
- [29] Kumar, G. & Garland, M. Visual exploration of complex time-varying graphs. *IEEE Transactions on Visualization & Computer Graphics* 805–812 (2006).
- [30] Loubier, E. & Dousset, B. Temporal and relational data representation by graph morphing. *Safety and Reliability for managing Risk (ESREL 2008), Hammamet* **14**, 2008–16 (2008).
- [31] Brandes, U., Indlekofer, N. & Mader, M. Visualization methods for longitudinal social networks and stochastic actor-oriented modeling. *Social Networks* **34**, 291–308 (2012).
- [32] Nguyen, Q., Eades, P. & Hong, S.-H. Streameb: Stream edge bundling. In *International Symposium on Graph Drawing*, 400–413 (Springer, 2012).
- [33] Federico, P. & Miksch, S. Evaluation of two interaction techniques for visualization of dynamic graphs. In *Graph Drawing and Network Visualization - 24th International Symposium, GD 2016, Athens, Greece, September 19-21, 2016, Revised Selected Papers*, 557–571 (2016). URL https://doi.org/10.1007/978-3-319-50106-2_43.

- [34] Nesbitt, K. V. & Friedrich, C. Applying gestalt principles to animated visualizations of network data. In *Information Visualisation, 2002. Proceedings. Sixth International Conference on*, 737–743 (IEEE, 2002).
- [35] Friedrich, C. & Eades, P. The marey graph animation tool demo. In *International Symposium on Graph Drawing*, 396–406 (Springer, 2000).
- [36] Hurter, C., Ersoy, O. & Telea, A. Graph bundling by kernel density estimation. In *Computer Graphics Forum*, vol. 31, 865–874 (Wiley Online Library, 2012).
- [37] Simonetto, P., Archambault, D. W. & Kobourov, S. G. Drawing dynamic graphs without timeslices. In *Graph Drawing and Network Visualization - 25th International Symposium, GD 2017, Boston, MA, USA, September 25-27, 2017, Revised Selected Papers*, 394–409 (2017). URL https://doi.org/10.1007/978-3-319-73915-1_31.
- [38] Pfitzner, R., Scholtes, I., Garas, A., Tessone, C. J. & Schweitzer, F. Betweenness preference: Quantifying correlations in the topological dynamics of temporal networks. *Phys. Rev. Lett.* **110**, 198701 (2013). URL <http://link.aps.org/doi/10.1103/PhysRevLett.110.198701>. <https://doi.org/10.1103/PhysRevLett.110.198701>.
- [39] Greilich, M., Burch, M. & Diehl, S. Visualizing the evolution of compound digraphs with timearctrees. In *Computer Graphics Forum*, vol. 28, 975–982 (Wiley Online Library, 2009).
- [40] Burch, M. & Diehl, S. Timeradartrees: Visualizing dynamic compound digraphs. In *Computer Graphics Forum*, vol. 27, 823–830 (Wiley Online Library, 2008).
- [41] Burch, M., Beck, F. & Weiskopf, D. Radial edge splatting for visualizing dynamic directed graphs. In *GRAPP/IVAPP*, 603–612 (2012).
- [42] Vehlow, C., Burch, M., Schmauder, H. & Weiskopf, D. Radial layered matrix visualization of dynamic graphs. In *2013 17th International Conference on Information Visualisation*, 51–58 (2013).
- [43] van den Elzen, S., Holten, D., Blaas, J. & van Wijk, J. J. Dynamic network visualization with extended massive sequence views. *IEEE Transactions on Visualization & Computer Graphics* 1087–1099 (2014).
- [44] Rosvall, M., Esquivel, A. V., Lancichinetti, A., West, J. D. & Lambiotte, R. Memory in network flows and its effects on spreading dynamics and community detection. *Nature communications* **5** (2014).
- [45] Xu, J., Wickramaratne, T. L. & Chawla, N. V. Representing higher-order dependencies in networks. *Science Advances* **2** (2016). URL <http://advances.sciencemag.org/content/2/5/e1600028>. <http://advances.sciencemag.org/content/2/5/e1600028.full.pdf>.
- [46] Mucha, P. J., Richardson, T., Macon, K., Porter, M. A. & Onnela, J.-P. Community structure in time-dependent, multiscale, and multiplex networks. *science* **328**, 876–878 (2010).
- [47] Mellor, A. The temporal event graph. *Journal of Complex Networks* **6**, 639–659 (2017).
- [48] Kivelä, M., Cambe, J., Saramäki, J. & Karsai, M. Mapping temporal-network percolation to weighted, static event graphs. *Scientific reports* **8**, 12357 (2018).
- [49] Salnikov, V., Cassese, D. & Lambiotte, R. Simplicial complexes and complex systems. *European Journal of Physics* **40**, 014001 (2018).

- [50] Scholtes, I. *et al.* Causality-driven slow-down and speed-up of diffusion in non-markovian temporal networks. *Nature Communications* **5**, 5024 (2014). URL <http://www.nature.com/ncomms/2014/140924/ncomms6024/full/ncomms6024.html>. <https://doi.org/10.1038/ncomms6024>, 1307.4030.
- [51] Scholtes, I., Wider, N. & Garas, A. Higher-order aggregate networks in the analysis of temporal networks: path structures and centralities. *The European Physical Journal B* **89**, 61 (2016). URL <http://dx.doi.org/10.1140/epjb/e2016-60663-0>. <http://dx.doi.org/10.1140/epjb/e2016-60663-0>.
- [52] Petrovic, L. V. & Scholtes, I. Counting causal paths in big times series data on networks. *arXiv preprint arXiv:1905.11287* (2019).
- [53] LaRock, T. *et al.* Detecting path anomalies in time series data on networks. *arXiv preprint arXiv:1905.10580* (2019).
- [54] Vaccario, G., Verginer, L. & Schweitzer, F. The mobility network of scientists: Analyzing temporal correlations in scientific careers. *arXiv preprint arXiv:1905.06142* (2019).
- [55] Isella, L. *et al.* What's in a crowd? analysis of face-to-face behavioral networks. *Journal of theoretical biology* **271**, 166–180 (2011).
- [56] Vanhems, P. *et al.* Estimating potential infection transmission routes in hospital wards using wearable proximity sensors. *PLoS ONE* **8** (2013).
- [57] Génois, M. *et al.* Data on face-to-face contacts in an office building suggest a low-cost vaccination strategy based on community linkers. *Network Science* **3**, 326–347 (2015).
- [58] Peixoto, T. P. & Rosvall, M. Modelling sequences and temporal networks with dynamic community structures. *Nature communications* **8**, 582 (2017).
- [59] Shewchuk, J. R. Adaptive precision floating-point arithmetic and fast robust geometric predicates. *Discrete and Computational Geometry* **18**, 305–363 (1997).

Supplementary Information

Vincenzo Perri¹ and Ingo Scholtes²

Data Analytics Group
Department of Informatics (IfI)
University of Zurich
Zürich, Switzerland

¹perri@ifi.uzh.ch, ²scholtes@ifi.uzh.ch

In this appendix, we provide supplementary information to (i) ensure the reproducibility of our experimental results, (ii) formally define (and illustrate) the layout quality measures used in section 4, and (iii) further back up our claims regarding the benefits of higher-order time-aware layouts of dynamic graphs.

A Model for Dynamic Graphs with Temporal Clusters

We provide additional details on the stochastic model used to generate synthetic dynamic graphs with temporal cluster structure and a random time-aggregated topology. The model performs the following three steps:

1. Generate a static random k -regular graph with n vertices, where each vertex is connected to a random set of k neighbours. Randomly assign the n vertices to three equally-sized, non-overlapping clusters, where $C(v)$ denotes the cluster of vertex v .
2. Generate N sequences of two randomly chosen time-stamped edges $(v_0, v_1; t)$ and $(v_1, v_2; t+1)$ that contribute to a causal path of length two in the resulting dynamic graph.
3. For each vertex v_1 of such a causal path of length two randomly pick:
 - two time-stamped edges $(u, v_1; t_1)$ and $(v_1, w, t_1 + 1)$ such that $C(u) = C(v_1) \neq C(w)$
 - two time-stamped edges $(x, v_1; t_2)$ and $(v_1, z; t_2 + 1)$ with $C(v_1) = C(z) \neq C(x)$
4. Swap the time stamps of the four time-stamped edges to $(u, v_1; t_1)$ and $(v_1, z; t_1+1)$, (x, v_1, t_2) , and $(v_1, w, t_2 + 1)$.

Steps 3 and 4 of this procedure exclusively change the temporal ordering of time-stamped edges in the dynamic graph generated in steps 1 and 2, affecting neither the topology nor the frequency of time-stamped edges. The model changes time stamps of edges (and thus causal paths) such that vertices are preferentially connected—via causal paths of length two—to other vertices in the same cluster. This leads to a strong cluster structure in the causal topology of the dynamic graph, which (i) is neither present in the time-aggregated topology nor in the temporal activation patterns of edges, and (ii) can nevertheless be visualised by our time-aware graph visualisation algorithm (see fig. 2 in main text).

An interactive HTML animation of a dynamic graph generated by this model and an interactive demo of the resulting time-aware static visualisation are available online². In fig. 2 we compare the layouts of the time-aggregated version of such a dynamic graph with a shuffled version. For this shuffling, we repeatedly pick pairs of time-stamped edges uniformly at random and swap their time stamps.

²see <http://www.pathpy.net/clustering.html>

B Quantitative Measures of Layout Quality

In the following, we provide formal definitions of the quantitative measures of layout quality, which we have introduced and used in section 4. For the following definitions, let $G^{(t)}$ be a dynamic graph that gives rise to a multi-set S of N causal paths $S = \{p_0, \dots, p_N\}$. We further assume that the time-aware layout algorithm presented in algorithm 1 assigns each vertex $v \in V$ to a position $\pi_v := Pos[v] \in \mathbb{R}^2$. Finally, we denote the time-aggregated static graph corresponding to the dynamic graph $G^{(t)}$ as $G = (V, E)$ (cf. definition in section 2.1). Using this terminology, we define the following measures:

Edge crossing (ξ) We define ξ as the number of times the visual representations of pairs of edges in terms of two-dimensional line segments in the graph layout cross each other.

We use a definition for edge crossing based on the well-known orientation predicate, which can be computed efficiently [59]. For an ordered sequence of three points $a = (a_x, a_y), b = (b_x, b_y), c = (c_x, c_y) \in \mathbb{R}^2$, it returns whether point c is on the “left-hand” or “right-hand” side of the plane defined by the vector \vec{ab} . This is equivalent to the question whether the points a, b and c are listed in “clockwise” or “counter-clockwise” order. Formally, the orientation predicate $orient(a, b, c)$ can be defined based on the determinant of a 3×3 matrix as:

$$orient(a, b, c) = \text{sign}((b_x - a_x) \cdot (c_y - a_y) - (c_x - a_x) \cdot (b_y - a_y))$$

where a positive value of $orient(a, b, c)$ indicates that c lies on the left-hand side of \vec{ab} , negative values indicate that c lies on the right-hand side of \vec{ab} , and zero indicates that a, b and c are co-linear.

With this auxiliary function, two edges $e_1 = (a, b)$ and $e_2 = (c, d)$ cross each other iff

$$orient(a, b, c) \neq orient(a, b, d) \text{ and } orient(c, d, a) \neq orient(c, d, b).$$

Causal path crossing (Ξ) Considering the time-stamped edges of a dynamic graph as causal paths of length one (cf. section 2.1), we generalise the notion of a crossing between two edges e_1 and e_2 to a crossing between two causal paths $p_1 = \overrightarrow{v_0 \dots v_l}$ and $p_2 = \overrightarrow{w_0 \dots w_m}$. Those two causal paths define a sequence of edges (v_i, v_{i+1}) ($i = 0, \dots, l - 1$) and (w_j, w_{j+1}) ($j = 0, \dots, m - 1$). We first say that there is a crossing between p_1 and p_2 if edge (v_i, v_{i+1}) crosses edge (w_j, w_{j+1}) for any pair of i and j . While this is a (trivial) generalisation of edge crossing to causal paths, we highlight non-trivial situations where causal paths traverse a common set of edges. In such situations, we can have a crossing between two causal paths despite not having a crossing between any pair of edges. An example of such a situation is shown in fig. 5.

To formally define our notion of path crossing in such non-trivial settings, we assume that p_1 and p_2 share a common sequence of vertices. Without loss of generality, let $s = \overrightarrow{x_0 \dots x_k}$ be a *common (sub)path*, consisting of a sequence of k shared vertices, where x_0 is the first shared vertex and x_k is the last shared vertex of the common path. We call the first and last vertex in such a subpath *junction vertices* at which the paths p_1 and p_2 either “join” or “fork”. Our notion of crossing between two causal paths with a common subpath can be illustrated in terms of two intersecting (directional) traffic flows in a network of road segments. As an example, consider the two causal paths \overrightarrow{ACDEFH} and \overrightarrow{BCDEFG} in fig. 5. Those two causal paths traverse the common subpath $s = \overrightarrow{CDEF}$ with junction vertices C and F . Let us now imagine two cars that follow those two paths, entering junction vertex C from vertex A and B respectively. From the perspective of car 1 entering C from vertex A on the purple path, the second car 2 enters C from the right-hand side on the green path. Both cars can continue along the common subpath \overrightarrow{CDEF} without having to cross each others’ “lanes”. At the junction vertex F , car 1 following the purple path continues to vertex H , exiting the joint path at the right-hand side. Car 2 following the green path continues towards G , exiting at the left-hand side. Since the enter and exit directions of the green and purple path have changed, we say that those two paths cross each other (at the junction vertex F).

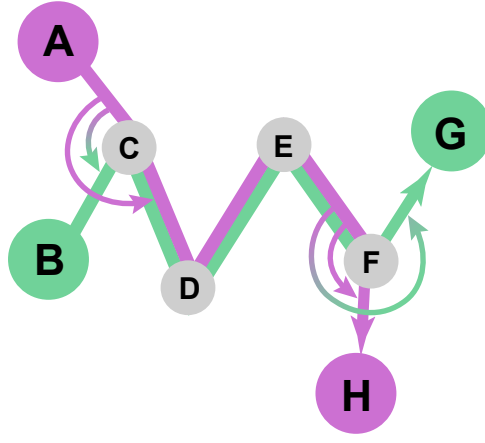


Figure 5: Illustration of path crossing Ξ . Due to the spatial positioning of the eight nodes in the example above, the two causal paths \overrightarrow{ACDEFH} (purple) and \overrightarrow{BCDEFG} (green) in this example cross each other at a junction vertex F .

Formally, we test for a crossing of two causal paths $p_1 = \overrightarrow{v_0 \dots v_l}$ and $p_2 = \overrightarrow{w_0 \dots w_m}$ by first calculating the set of common subpaths $X = \{s_1, \dots, s_N\}$. Consider an element (subpath) $s = \overrightarrow{x_0 \dots x_k}$ of X . If (v_i, x_0) and (w_j, x_0) for some i and j , we have the case that p_1 and p_2 “enter” s at the junction vertex x_0 , continuing to x_1 . We then consider two pairs of line segments (x_0, v_i) , (x_0, x_1) and (x_0, w_j) , (x_0, x_1) and calculate the angles $\Theta_1(x_0)$ and $\Theta_2(x_0)$ between them respectively as

$$\Theta_1(x_0) := \arccos\left(\frac{\overrightarrow{x_0 v_i} \cdot \overrightarrow{x_0 x_1}}{\|\overrightarrow{x_0 v_i}\| \cdot \|\overrightarrow{x_0 x_1}\|}\right), \Theta_2(x_0) := \arccos\left(\frac{\overrightarrow{x_0 w_j} \cdot \overrightarrow{x_0 x_1}}{\|\overrightarrow{x_0 w_j}\| \cdot \|\overrightarrow{x_0 x_1}\|}\right)$$

Note that \arccos yields radial angles in $[0, \pi]$, i.e. we necessarily obtain angles smaller than π . To obtain angles in the interval $[0, 2\pi]$, we use the orientation predicate, and take the complementary angles $2\pi - \Theta_1(x_0)$ and $2\pi - \Theta_2(x_0)$ of $\Theta_1(x_0)$ and $\Theta_2(x_0)$ if the three points are given in counter-clockwise order, i.e. if the orientation predicate yields -1 .

We use $\Theta_1(x_0)$ and $\Theta_2(x_0)$ to determine in which spatial orientation paths enter the joint path segments s at junction vertex x_0 . If $\Theta_1(x_0) - \Theta_2(x_0) > 0$ we have that—from the perspective of p_1 — p_2 enters junction vertex x_0 from the right, while for $\Theta_1(x_0) - \Theta_2(x_0) < 0$ it enters from the left (see angles $\Theta_1(x_0)$ and $\Theta_2(x_0)$ around vertex C indicated by circular arrows in fig. 5).

Analogously to the case of two paths *entering* a junction vertex x_0 , if (x_k, v_i) and (x_k, w_j) for some i and j we have the case that p_1 and p_2 *exit* the common subpath s at vertex x_k , continuing to v_i and w_j respectively. Here we calculate the angles $\Theta_1(x_k)$ and $\Theta_2(x_k)$ between pairs of line segments (x_k, v_i) , (x_k, x_{k-1}) and (x_k, w_j) , (x_k, x_{k-1}) respectively as

$$\Theta_1(x_k) := \arccos\left(\frac{\overrightarrow{x_k v_i} \cdot \overrightarrow{x_k x_{k-1}}}{\|\overrightarrow{x_k v_i}\| \cdot \|\overrightarrow{x_k x_{k-1}}\|}\right), \Theta_2(x_k) := \arccos\left(\frac{\overrightarrow{x_k w_j} \cdot \overrightarrow{x_k x_{k-1}}}{\|\overrightarrow{x_k w_j}\| \cdot \|\overrightarrow{x_k x_{k-1}}\|}\right)$$

again using the orientation predicate to obtain radial angles in the range $[0, 2\pi]$. If $\Theta_1(x_k) - \Theta_2(x_k) > 0$ we have that—from the perspective of p_1 —the path p_2 *exits* the junction vertex x_k to the right, while for $\Theta_1(x_k) - \Theta_2(x_k) < 0$ path p_2 exists to the left (see angles around vertex F indicated in fig. 5).

Using the definitions above, we say that there is a crossing between two causal paths p_1 and p_2 iff (i) they contain a pair of crossing edges, or (ii) there is a common subpath $s = \overrightarrow{x_0 \dots x_k}$ such that $\exists t : \text{sign}(\Theta_1(x_0) - \Theta_2(x_0)) \neq \text{sign}(\Theta_1(x_k) - \Theta_2(x_k))$, i.e. we have the situation that p_1 and p_2 enter and exit p_x at opposite sides. Using this approach, in the example shown in fig. 5 for the two paths $p_1 = \overrightarrow{ACDEFH}$ and $p_2 = \overrightarrow{BCDEFG}$ with common subpath $s = \overrightarrow{CDEF}$ we first identify

the junction vertices C and F and then compute the angles Θ_1 and Θ_2 for those junction vertices. In the example, we find that $\Theta_1(C) - \Theta_2(C) > 0$ while $\Theta_1(F) - \Theta_2(F) < 0$, which confirms that p_1 and p_2 cross each other at vertex F .

Causal path dispersion (σ) We define a measure of causal path dispersion σ that captures to what extent the vertices traversed by causal paths are more or less spatially distributed than expected based on the spatial distribution of all vertices. For a multi-set S of causal paths p with cardinality $N := |S|$ traversing a graph with vertices V we define σ as

$$\sigma = \sum_{p \in S} \frac{B(\{v_i \in p\})}{N \cdot B(V)},$$

where $B : 2^V \rightarrow \mathbb{R}^2$ is a function that returns the barycentre of vertex positions for a multi-set V' of vertices, i.e.

$$B(V') := \frac{1}{|V'|} \sum_{v \in V'} \text{Pos}[v].$$

Figure 6 shows an example for a causal path that illustrates the definition of causal path dispersion. In this example, the positions of vertices on the two causal paths $\overrightarrow{ABCD\hat{A}}$ (purple) and \overrightarrow{EFG} (green) are less spatially dispersed than expected considering the spatial distribution of all vertices.

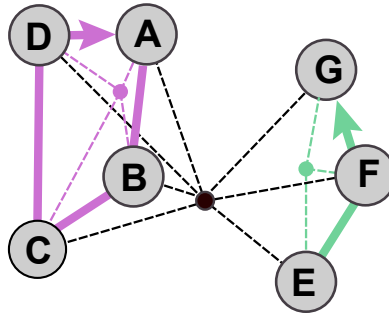


Figure 6: Illustration of *causal path dispersion* σ . Dotted lines indicate the distances of the vertices traversed by two causal paths $\overrightarrow{ABCD\hat{A}}$ (purple) and \overrightarrow{EFG} (green) from the barycentre of all vertices (black dot) and the barycentre of vertices on individual paths (colored dots).

Closeness eccentricity (Δ) We finally define a measure that captures to what extent vertices that are positioned close to the centre of a (time-aggregated) graph visualisation have high temporal closeness centrality in the underlying dynamic graph. For a set S of causal paths p in a dynamic graph, we first define the temporal closeness centrality of vertex v as

$$CC(v) := \sum_{w \neq v \in V} \frac{\sum_{p \in S} \delta_w(p) \delta_v(p)}{\sum_{p \in S, w \in p} \text{dist}(v, w; p)}$$

where we define $\text{dist}(v, w; p)$ as the (topological) distance between vertices v and w via causal path p and $\delta_v(p)$ is one if path p traverses vertex v and zero otherwise. With (x, y) being the barycentre of vertex positions $\text{Pos}[v]$ in the visualisation of the dynamic graph, for a given number n of vertices with highest temporal closeness centrality, we define $\Delta(n)$ as

$$\Delta(n) := \frac{\sum_{i=1}^n \|\text{Pos}[u_i] - (x, y)\| \cdot |V|}{n \cdot \sum_{v \in V} \|\text{Pos}[v] - (x, y)\|}$$

where u_1, u_2, \dots, u_n are the n most central vertices. We note that values of $\delta(n)$ larger or smaller than one capture whether the n vertices with highest temporal closeness centrality are closer to ($\Delta < 1$) or farther away from ($\Delta > 1$) the barycentre of the time-aggregated graph visualisation than we would expect at random.

Figure 7 shows an illustrative example of closeness eccentricity for a standard (time-neglecting) force-directed layout (left) and a time-aware layout (right) of the same dynamic graph. The size of vertices in both visualisations is proportional to their temporal closeness centrality in the underlying dynamic graph. We have further highlighted the $n = 3$ most central vertices in red. In both graph drawings, the black dot represents the barycentre of all vertex positions, while dotted lines indicate the distance of the three most central vertices from the barycentre. The average distance of the three most central vertices in the time-neglecting layout shown in the left is not substantially different from the average distance of all vertices from the barycentre, thus resulting in a value of $\Delta \approx 1$. For the time-aware layout computed with HOTVis (right), the average distance of the vertices with highest temporal closeness centrality from the barycentre is smaller than the average distance of all vertices, thus resulting in $\Delta < 1$.

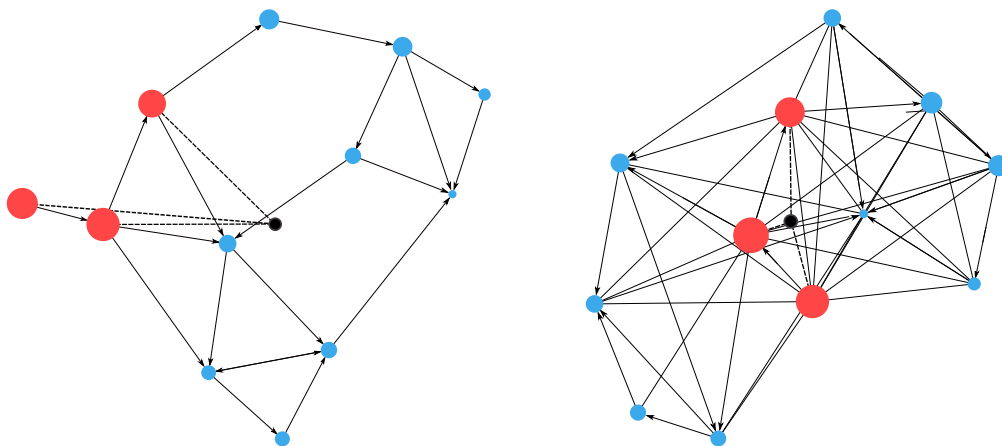


Figure 7: Comparison of closeness eccentricity in a standard time-neglecting force-directed layout (left) and a time-aware layout generated by HOTVis. Size of vertices are proportional to their *temporal* closeness centrality in the underlying dynamic graph, where the $n = 3$ most central vertices are shown in red. In the time-ware layout generated by HOTVis, vertices with high temporal closeness centrality are positioned relatively closer to the barycentre of the visualisation than other vertices.

C Supplementary Results

Here we present additional quantitative results that support our claim that the time-aware visualisation technique proposed in our manuscript highlights important temporal patterns in dynamic graphs. Due to space limitations, those results could not be included in the main text.

The scatter plots in fig. 8 show the number of causal paths (of any length) existing between pairs of vertices (on the x-axis) as well as the spatial distances between those pairs of vertices in a static graph visualisation (y-axis) in a synthetically generated dynamic graph. This dynamic graph was generated using the stochastic model described in appendix A, i.e. the generated dynamic graph exhibits three temporal clusters, where each cluster contains ten vertices (cf. fig. 2 in main text). Pairs of vertices that are members of the same clusters are shown in pink. Pairs of vertices in different clusters are shown in blue. The left panel in fig. 8 shows the scatter plot for a (time-ignoring) static, first-order visualisation, where the positions of vertices are exclusively generated based on the static graph topology. The right panel shows the same plot for a second-order time-aware visualisation generated by our proposed algorithm HOTVis. A clear difference is visible in those plots, showing that our time-aware visualisation approach tends to position those pairs of vertices in closer proximity

that are connected by a larger number of causal paths. Conversely, nodes that are less connected by causal paths than expected from the static topology are placed at larger distance in the static visualisations. This result confirms the visual impression in fig. 2 in the main text, that the time-aware layout highlights cluster structures in the causal topology.

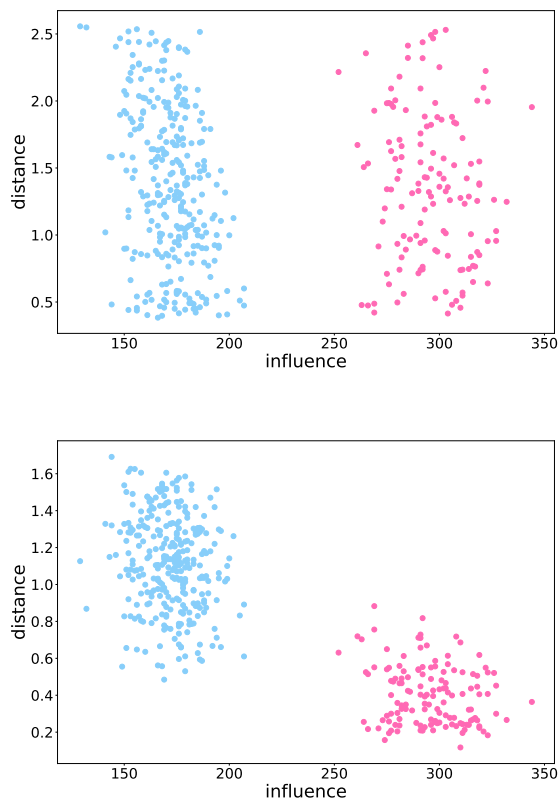


Figure 8: Scatter plot showing the number of causal paths (of any length) existing between pairs of vertices (x-axis) and the spatial distance between all pairs of vertices (y-axis) in two static visualisations of a dynamic graph with temporal communities that was generated as described in appendix A. Pairs of vertices in the same clusters are shown in pink, while pairs of vertices in different clusters are shown in blue. The top panel shows the results for a (time-neglecting) first-order layout, while the bottom panel shows a second-order time-aware visualisation generated by HOTVis.

D Notes on Computational Complexity

We briefly comment on the computational complexity of HotVis. We first note that the complexity of the second phase of algorithm 1 in the main text corresponds to the computational complexity of the well-known force-directed layout algorithm introduced in [19]. The additional computational effort that is introduced in the first phase of our algorithm directly depends on the computational complexity of generating k -th order graph models for $k = 2, \dots, K$. While we refer the reader to [52] for a detailed discussion (and proof) of the complexity of generating higher-order models of causal paths of length k , here we highlight that a term for the worst-case complexity can be given as

$$\mathcal{O}(N \cdot |V| \cdot K^2 \cdot [m\delta\lambda_{\max}^{K-2} + \lambda_{\max}]),$$

where N is the number of time-stamped edges in the dynamic graph, $|V|$ is the number of vertices, K is the maximum order of the higher-order graph model used in the time-aware visualisation, m is the maximum number of time-stamped edges with the same time stamp, δ is the maximum time

difference used in the definition of causal paths, and λ_{\max} is the largest eigenvalue of the binary adjacency matrix of the time-aggregated graph topology [52, 53].

This result shows that the computational complexity of our visualisation algorithm strongly depends on the temporal distribution of time-stamped edges, which influences the number of causal paths of length k and thus the size of a k -th order graph. Moreover, the scaling of computational complexity with the maximum order K that is used in the visualisation depends on the sparsity of the time-aggregated topology expressed in the leading eigenvalue λ_{\max} of the adjacency matrix.

For empirical data, we find that higher-order graph models are generally highly sparse, which enables us to compute higher-order time-aware graph layouts up to a maximum order $K \approx 10$ in a few seconds even for data on dynamic graphs with millions of time-stamped edges.

E Software Implementation and Reproducibility

The proposed algorithm `HOTVis`, as well as the quality measures described in appendix B have been implemented in the OpenSource python data analytics and visualisation package `pathpy` [12]. Interactive tutorials, animations, and illustrative examples that showcase our concept of higher-order time-aware layouts of dynamic graphs, and their implementation in the python package `pathpy` are available online at www.pathpy.net. The empirical time-stamped social networks that were used in this work are freely accessible at www.sociopatterns.org. A tutorial that shows how to analyse those two data sets with `pathpy` is available at www.pathpy.net.